Great Salt Lake–Effect Precipitation: Observed Frequency, Characteristics, and Associated Environmental Factors

TREVOR I. ALCOTT AND W. JAMES STEENBURGH

Department of Atmospheric Sciences, University of Utah, Salt Lake City, Utah

NEIL F. LAIRD

Hobart and William Smith Colleges, Geneva, New York

(Manuscript received 6 February 2012, in final form 16 March 2012)

ABSTRACT

This climatology examines the environmental factors controlling the frequency, occurrence, and morphology of Great Salt Lake–effect (GSLE) precipitation events using cool season (16 September–15 May) Weather Surveillance Radar-1988 Doppler (WSR-88D) imagery, radiosonde soundings, and MesoWest surface observations from 1997/98 to 2009/10. During this period, the frequency of GSLE events features considerable interannual variability that is more strongly correlated to large-scale circulation changes than lake-area variations. Events are most frequent in fall and spring, with a minimum in January when the climatological lake surface temperature is lowest. Although forecasters commonly use a 16°C lake–700-hPa temperature difference (ΔT) as a threshold for GSLE occurrence, GSLE was found to occur in winter when ΔT was only 12.4°C. Conversely, GSLE is associated with much higher values of ΔT in the fall and spring. Therefore, a seasonally varying threshold based on a quadratic fit to the monthly minimum ΔT values during GSLE events is more appropriate than a single threshold value. A probabilistic forecast method based on the difference between ΔT and this seasonally varying threshold, 850–700-hPa relative humidity, and 700-hPa wind direction offers substantial improvement over existing methods, although forecast skill is diminished by temperature and moisture errors in operational models. An important consideration for forecasting because of their higher precipitation rates, banded features—with a horizontal aspect ratio of 6:1 or greater—dominate only 20% of the time that GSLE is occurring, while widespread, nonbanded precipitation is much more common. Banded periods are associated with stronger low-level winds and a larger lake–land temperature difference.

1. Introduction

Lake- and ocean-effect precipitation occurs across the globe on a wide range of spatial scales, from the Sea of Japan (e.g., Kusunoki et al. 2004), the North Channel (e.g., Browning et al. 1985), and the Laurentian Great Lakes (e.g., Braham and Dungey 1984; Niziol 1987; Niziol et al. 1995) to smaller water bodies like the Great Salt Lake (e.g., Carpenter 1993; Steenburgh et al. 2000), Lake Champlain (e.g., Payer et al. 2007; Laird et al. 2009a), and the Finger Lakes (e.g., Laird et al. 2009b, 2010). These precipitation events occur when the interaction of a cold continental or Arctic air mass with a relatively warm body of water initiates or enhances moist convection. Although smaller water bodies have received more attention in the past decade (e.g., Steenburgh et al. 2000; Steenburgh and Onton 2001; Onton and Steenburgh 2001; Payer et al. 2007; Laird et al. 2009a,b, 2010), most lake-effect research has been concerned with the Laurentian Great Lakes (hereafter, the Great Lakes). In comparison, the Great Salt Lake (GSL) presents a unique situation where lake-effect events are associated with a meso-β-scale hypersaline lake adjacent to steep topographic barriers and a densely populated urban corridor. Past investigations of the GSL effect (GSLE) have been limited by the lack of radar data (i.e., Carpenter 1993) or a short study period (i.e., Steenburgh et al. 2000). GSLE storms remain a challenge to predict, and forecasters continue to struggle to identify the primary factors that contribute to their initiation and varied evolution.

A terminal lake, the GSL is approximately 120 km by 45 km, with a maximum depth of only 10 m, and an area ranging from 2500 to 8500 km^2 over the past

Corresponding author address: Trevor Alcott, Dept. of Atmospheric Sciences, University of Utah, 135 S. 1460 E., Rm. 819, Salt Lake City, UT 84112-0110.
E-mail: trevor.alcott@utah.edu

DOI: 10.1175/WAF-D-12-00016.1

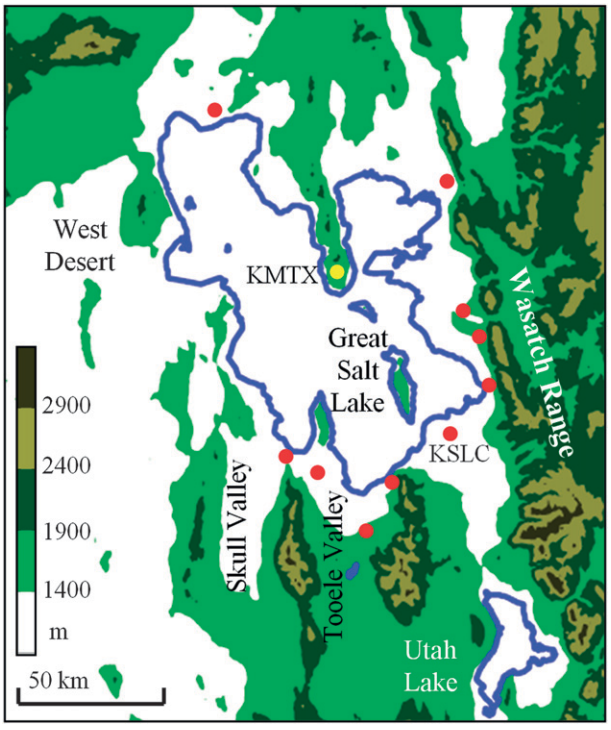

FIG. 1. Topography and landmarks of the study region; red dots mark the locations of mesonet stations used in the calculation of $\Delta T_{\text{LAKE–LAND}}$.

half-century, approximately 1/30th to 1/10th the area of Lake Superior (Fig. 1; USGS 2012). Despite the relatively small size of the GSL, multiple lake-effect precipitation events occur annually. These events can reduce visibilities to 1/4 mi (400 m) or less, and have produced snow accumulations of over 60 cm at both valley and mountain sites (e.g., Carpenter 1993; Steenburgh et al. 2000; Steenburgh 2003). The GSL is flanked on its east and south shores by Interstates 15 and 80, respectively, and the adjacent Wasatch Front urban corridor has a population of more than 1.5 million (U.S. Census Bureau 2011).

Several factors contribute to the development of lake-effect precipitation over the Great Lakes—including a stationary or slow-moving 500-hPa low to the north, a strong flow of relatively cold air over the lakes, a long fetch, and a sufficient temperature differential between the low-level air mass and the lakes (Wiggin 1950; Niziol 1987; Niziol et al. 1995). Steenburgh et al. (2000) found analogous conditions in GSLE events, with precipitation accompanied by a lake–700-hPa temperature difference of at least 16°C (approximately equivalent to a dry-adiabatic lapse rate), a lack of stable layers below 700 hPa, weak low-level directional shear (<60° in the 800–600-hPa layer, with the GSL at ~870 hPa), and a large lake–land temperature difference, the latter favoring land-breeze convergence over the GSL. Although Steenburgh et al. (2000) established a parameter space in which GSLE events can occur, they did not attempt to differentiate between the conditions associated with GSLE and non-GSLE periods.

Near the Great Lakes, lake-effect precipitation has been classified using the following morphological categories: 1) widespread coverage of wind-parallel horizontal roll convection (e.g., Kristovich and Laird 1998), 2) shoreline bands (e.g., Hjelmfelt and Braham 1983), 3) solitary midlake bands (e.g., Passarelli and Braham 1981), and 4) mesoscale vortices (e.g., Laird 1999). Laird et al. (2003a) group shoreline and midlake bands together since both morphologies tend to occur with similar environmental conditions. Using a series of idealized model simulations, Laird et al. (2003b) identified the parameter U/L, the ratio of wind speed to fetch, as a discriminator between lake-effect morphologies. However, an investigation of historical lake-effect events in the Great Lakes showed U/L had somewhat limited value in discriminating observed events (Laird and Kristovich 2004). Steenburgh et al. (2000) found GSLE precipitation structures ranging from a broad area of precipitation southeast of the lake to a single narrow midlake band, with no cases of multiple wind-parallel bands such as those observed over the Great Lakes. It remains to be determined whether environmental factors can be used to discriminate morphological lake-effect transition zones on smaller lakes such as the GSL.

Our research seeks to better understand the environmental factors that affect the frequency, morphology, and coverage of GSLE precipitation, and differentiate between GSLE and non-GSLE periods, through the development and analysis of a 13-yr cool-season radar-derived climatology. We will show that GSLE events occur primarily within specific ranges of instability, moisture, and kinematic parameters, whereas considerable overlap exists between the conditions associated with different GSLE morphologies. Furthermore, we identify deficiencies in current forecast techniques and present a new probabilistic approach using lake–air temperature difference, low-level relative humidity, and wind direction.

2. Data and methods

a. Event identification

GSLE events were identified visually using lowest-tilt (0.5°) radar reflectivity images from the Weather Surveillance Radar-1988 Doppler (WSR–88D) at Promontory Point, Utah (KMTX; Fig. 1), for the cool seasons

(16 September–15 May) of 1997/98–2009/10. Radar data were obtained from the National Climatic Data Center Hierarchical Data Storage System, where temporal coverage was poor during 1994–96 and greatly improved by fall 1997. Hence, we began our examination later than Steenburgh et al. (2000), who used 1994/95–1997/98. Following Laird et al. (2009a), GSLE events were defined as periods ≥ 1 h where precipitation features were (a) coherent and quasi stationary with a distinct connection to the lake; (b) shallow and distinguishable from large, transitory ''synoptic'' features; and (c) exhibiting increasing depth and/or intensity in the downwind direction.

Although topography partially or completely blocks a large portion of the 0.5° radar tilt east of the Wasatch Range, horizontal coverage over the Great Salt Lake, northern Wasatch Front, and Salt Lake Valley is nearly uninhibited (Wood et al. 2003). Radar data are available in two forms, with base data in level II files and base and derived products in level III files (Crum et al. 1993). While level II data are frequently missing (for 14.9% of the time during the study period), level III data are missing for less than 3% of the time. Out of 3162 total days, 26 days (0.8%) contained both missing level II and III radar data for time periods longer than the average duration of a GSLE event (11.3 h).

TABLE 1. Sounding and surface variables used in the analysis.

Variable	Levels
Temperature, geopotential height, RH, zonal and meridional wind components, wind speed, wind direction, fetch, potential temperature, equivalent potential temperature, lake–air temperature difference	Surface, 850–100 hPa in 10-hPa intervals
Mean RH, mean wind speed, lapse rate, vertical gradient in potential temperature, vector wind shear magnitude, speed shear, directional shear	All 50–550-hPa intervals between 850 and 300 hPa
Locomotive Springs RH	2 m
Lake–land temperature difference (mean of 11 sites surrounding the GSL)	2 m

b. Surface and upper-air observations

Hourly surface observations were obtained from the MesoWest database at the University of Utah (Horel et al. 2002). Table 1 lists the basic and derived upper-air variables used in the analysis, all of which come from soundings launched by the National Weather Service Forecast Office at Salt Lake City International Airport (KSLC; see Fig. 1 for location). These data were obtained from the University of Wyoming archive and were interpolated to 10-hPa vertical intervals. A sounding is considered to be associated with GSLE if GSLE occurs within a 3-h window centered on the sounding time (e.g., at any point between 1030 and 1330 UTC for a 1200 UTC sounding). Of 5737 soundings analyzed, 140 were associated with GSLE (45 at 0000 UTC and 95 at 1200 UTC). The small size of this sample relative to the number of GSLE events reflects both the use of a narrow, 3-h window for verification, and the occurrence of some short-duration (<6 h) GSLE events. In the majority of GSLE events, KSLC was downstream of the GSL and the observed atmospheric profiles likely represent air in the lower troposphere that experienced some modification over the GSL. However, the nearest upstream upper-air observation sites (Boise, Idaho, and Elko, Nevada) are 250–350 km from the GSL and are of limited value due to the existence of intervening mountain ranges.

For two-dimensional analyses of the large-scale patterns associated with GSLE, upper-air composites of the GSLE environment were produced using data from the North American Regional Reanalysis (NARR; Mesinger et al. 2006), obtained from the National Climatic Data Center.

c. Event classification

Through visual inspection of radar images, we classified both the context (i.e., the general character of GSLE events relative to other precipitation features) and the morphology (i.e., the convective mode) of GSLE every 3 h. Context was classified as follows: 1) isolated areas of lake-effect precipitation, with no other precipitation falling in the surrounding valleys (i.e., pure lake effect), 2) lake-effect precipitation concurrent with other primarily convective precipitation features, 3) lake-effect precipitation concurrent but not collocated with synoptic/transient stratiform precipitation, and 4) localized lake enhancement of transient precipitation. Examples of these four categories are shown in Fig. 2. GSLE frequently coincides with orographic precipitation over the Wasatch and Oquirrh Mountains. No attempt was made to classify combined lake-orographic precipitation scenarios as a separate category, since nearby mountain ranges are often directly downstream of the GSL, and may be within a lake-effect precipitation structure.

GSLE morphology was classified as either 1) nonbanded, 2) mixed mode (i.e., primarily nonbanded with some banded features), or 3) banded (see examples in Fig. 3). Bands were defined as contiguous areas of

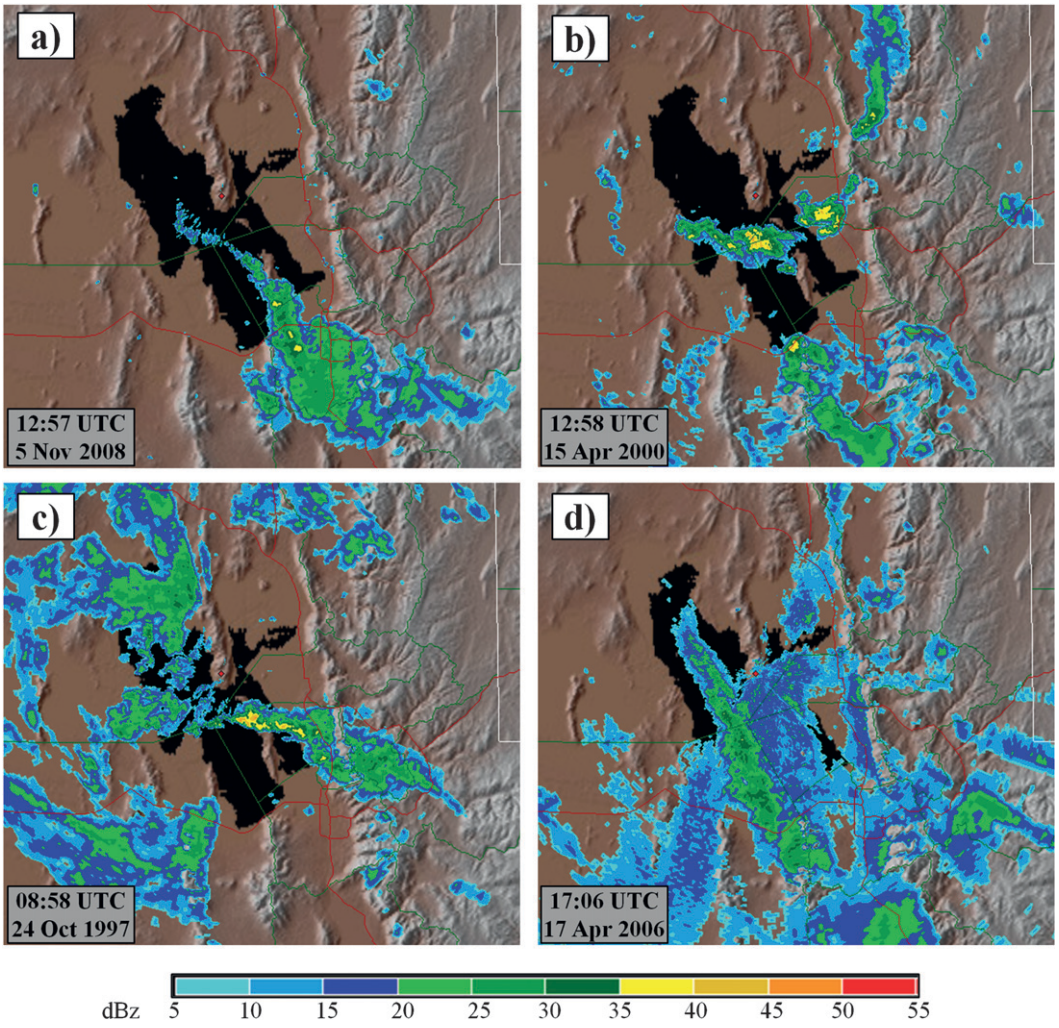

FIG. 2. Examples of GSLE precipitation context: (a) isolated areas of lake-effect precipitation, with no other precipitation falling in the surrounding valleys; (b) lake-effect precipitation concurrent with other primarily convective precipitation features; (c) lake-effect precipitation concurrent but not collocated with synoptic/transient stratiform precipitation; and (d) localized lake enhancement of transient precipitation.

reflectivity ≥ 10 dBZ with a horizontal aspect ratio of at least 6:1 (Weckwerth et al. 1997), which is approximately equal to the aspect ratio of the main body of the GSL, aiding visual classification of the radar data. While the morphology was determined every 3 h during GSLE events, analysis of the environmental conditions affecting the morphology was only performed for 3-h periods surrounding upper-air sounding launches at KSLC (e.g., 1030–1330 UTC for a 1200 UTC sounding).

d. Great Salt Lake temperature

A consistent record of daily GSL temperature observations does not currently exist. Steenburgh et al. (2000) used data from bimonthly U.S. Geological Survey (USGS) bucket samples to construct a climatological curve for GSL temperature. Crosman and Horel (2010) later applied cloud and land masks to surface temperature data from the Moderate Resolution Imaging Spectroradiometer (MODIS) and obtained a representative GSL temperature by calculating the median temperature of all unmasked pixels. Although an improvement over the use of bucket samples, MODIS temperature data were not available on many days due to frequent obscuration of the lake by clouds. Crosman and Horel (2010) constructed a curve similar to that of Steenburgh et al. (2000) by fitting a cosine function to points representing the average temperature of all available images in each month.

For this study, a third climatology curve was calculated by applying a Fourier fit between the Julian day and MODIS-observed temperatures in the Crosman and Horel (2010) dataset, given by

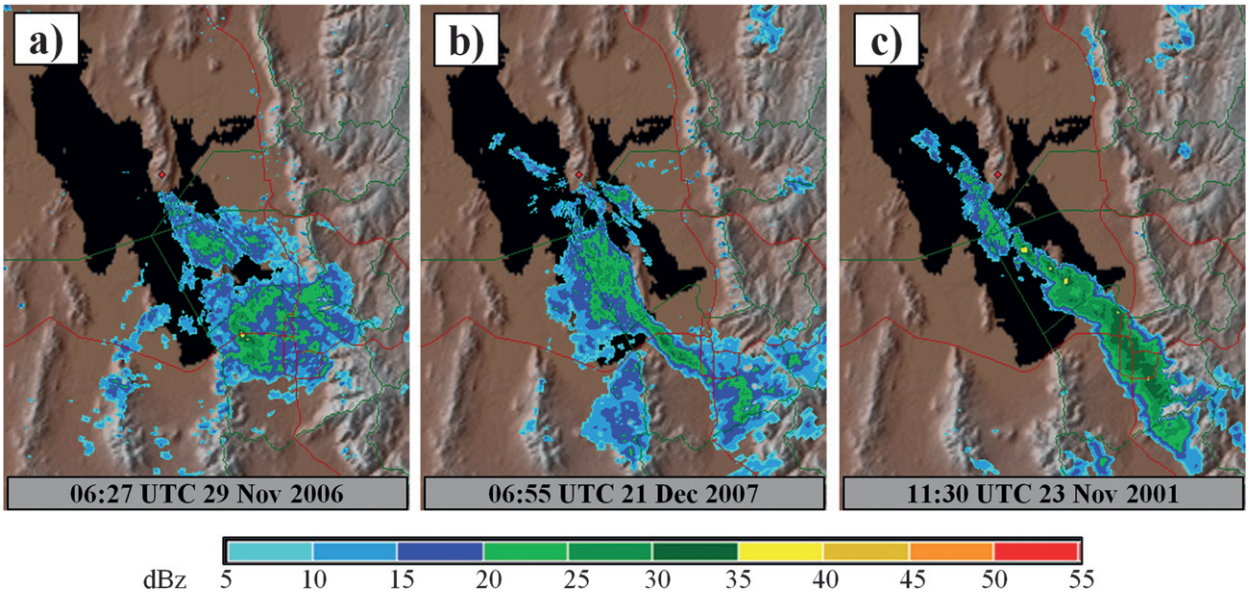

FIG. 3. Examples of GSLE morphology categories: (a) nonbanded, (b) mixed mode, and (c) banded.

$$T_{\text{LAKE-CLIMO}} = 13.8 - 11.9\cos(0.0172j) - 4.09\sin(0.017j) - 0.93\cos(0.0344j) + 0.677\sin(0.0344j) - 0.482\cos(0.0516j) - 0.600\sin(0.0516j),$$

where $T_{\text{LAKE-CLIMO}}$ is the climatological GSL temperature on Julian day j. This curve better captures the winter minimum and the rate of increase in spring (Fig. 4). The shallow waters of the GSL are prone to significant departures from climatology, as shown when MODIS-derived GSL temperatures [medians calculated as in Crosman and Horel (2010)] are compared to the three curve fits. To address this issue, we adapted the approach of Carpenter (1993) by calculating a linear relationship between the GSL temperature anomaly (relative to our Fourier fit climatology curve) and the anomaly in 7-day mean temperature at KSLC. KSLC 7-day mean temperature anomalies were computed relative to a Fourier fit estimation of the 1997–2010 KSLC temperature climatology, given by

$$T_{\text{KSLC-CLIMO}} = 11.3 - 13.4\cos(0.0167j) - 3.29\sin(0.0167j) + 0.472\cos(0.0334j) + 1.90\sin(0.0334j),$$

where $T_{\text{KSLC-CLIMO}}$ is the climatological 7-day mean temperature at KSLC ending on Julian day j. The relationship between GSL temperature and KSLC temperature,

$$T_{\text{LAKE}} = T_{\text{LAKE-CLIMO}} + 0.39(T_{\text{KSLC}} - T_{\text{KSLC-CLIMO}}),$$

where T_{LAKE} is the estimated GSL temperature, $T_{\text{LAKE-CLIMO}}$ is the climatological GSL temperature, T_{KSLC} is the 7-day mean temperature at KSLC, and $T_{\text{KSLC-CLIMO}}$ is the climatological 7-day mean temperature at KSLC, was calculated from a dependent set containing 80% of

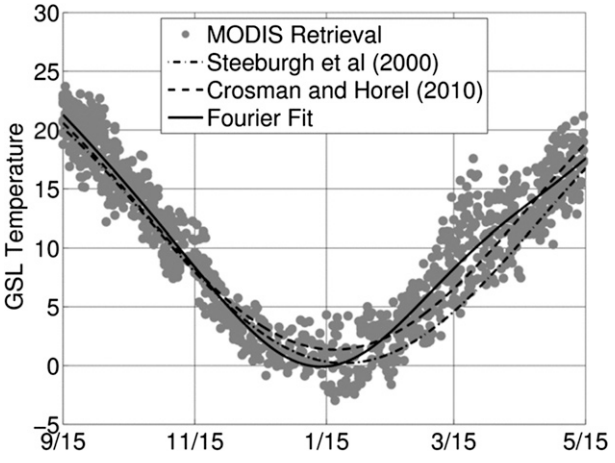

FIG. 4. MODIS GSL temperature vs three climatological curve fits.

TABLE 2. Performance of four methods for estimating GSL temperature, evaluated for an independent set of 240 MODIS overpasses.

T_{Lake} method	R^2	RMSE (°C)	Bias (°C)
Steenburgh et al. (2000)	0.88	7.06	−1.39
Crosman and Horel (2010)	0.90	4.35	−0.30
Fourier fit	0.92	3.51	−0.10
KSLC anomaly regression	0.95	2.31	−0.11

the 1700 MODIS images and then tested on an independent set containing the remaining 20%. This methodology yields a substantial improvement in GSL temperature estimation over any previous climatology curve (Table 2) and has been applied to the entire 13-cool-season study period to produce a continuous GSL temperature record. Errors in temperature estimation were less than 2°C in 82% of the independent test cases and were largest in spring when Crosman and Horel (2010) found the largest diurnal ranges. Most of the large regression errors in spring were daytime underestimates and nighttime overestimates.

3. Results

a. *Frequency, characteristics, and seasonality of GSLE events*

During the 13 cool seasons, 149 GSLE events were identified. The mean event duration was 11.3 h, although events lasted an average of 3.1 h longer in fall (16 September–30 November) and winter (1 December–28 February) than in spring (1 March–15 May). There were 11 events with durations ≥ 24 h, up to a maximum of 48 h during 25–27 November 2001. GSLE context was distributed as follows: isolated areas of lake-effect precipitation, 1780 h (62% of the time GSLE was observed); lake effect concurrent with other primarily convective precipitation features, 356 h (20%); lake effect concurrent but not collocated with synoptic/transient stratiform precipitation, 178 h (10%); and localized lake enhancement of transient precipitation, 142 h (8%).

There exists large interannual variability in event frequency, with the number of events per cool season averaging 13 but ranging from 3 to 20 (Fig. 5a). Cool seasons with fewer trough days (i.e., days when the 500-hPa relative vorticity exceeds 2×10^{-5} s^{-1} at Salt Lake City at 0000 and 1200 UTC) are generally marked by fewer GSLE events (Fig. 5b; shown as standardized anomalies, i.e., departures from the study period mean expressed as the number of the standard deviations; correlation coefficient $R = 0.64$), as are cool seasons with a lower mean lake–700-hPa temperature difference

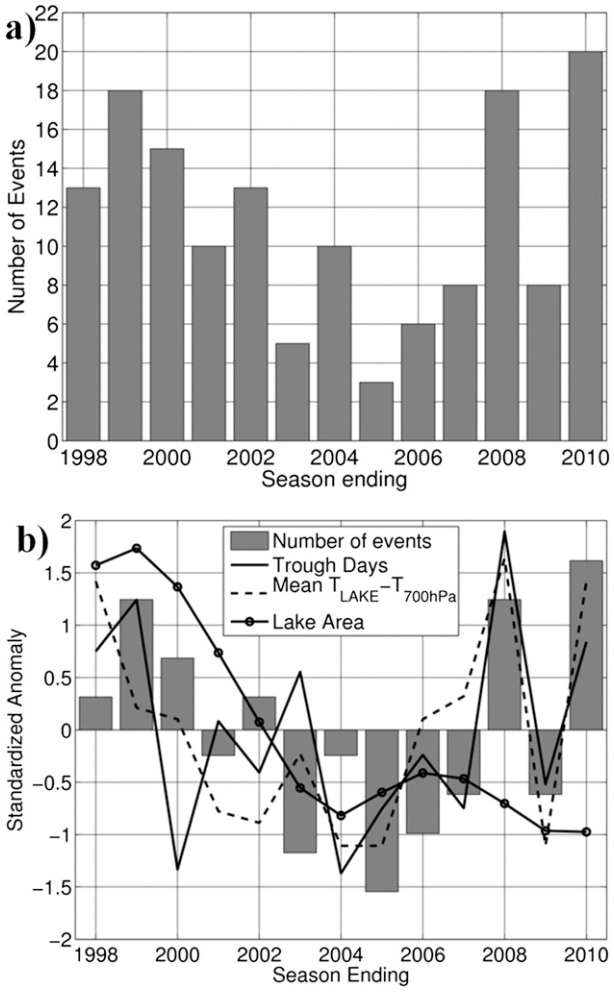

FIG. 5. (a) Annual frequency of GSLE events. (b) Standardized anomalies of event frequency, lake area, and synoptic factors.

($R = 0.62$). Although the sample size is small, the null hypothesis of zero true correlation can be rejected with at least 98% confidence ($P < 0.02$) for both of these factors. The GSL ranged in area between 3100 and 4500 km^2 over the study period (USGS 2012), but over this interval, the relationship between GSL area and GSLE frequency is weaker than for the aforementioned synoptic factors (Fig. 5b; $R = 0.34$, $P = 0.26$). These results suggest atmospheric factors have a larger impact on interannual variability in GSLE frequency than do fluctuations in the lake area. From 1861 to 2011, the area of the GSL varied between 2460 and 8550 km^2 (USGS 2012), a much larger range that could have had a more measureable effect on GSLE frequency, but an analogous event climatology does not exist for longer time periods.

The seasonal event distribution is bimodal, with the frequency highest from mid-October to mid-December

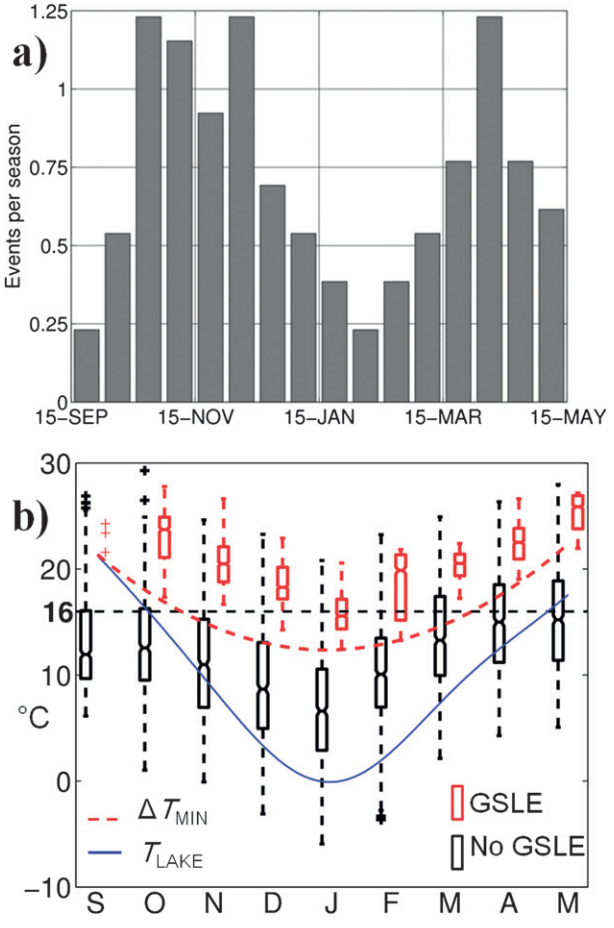

FIG. 6. (a) Number of events by half-month. (b) Standard box-and-whiskers plot of lake–700-hPa temperature difference (ΔT) by month, for non-GSLE (black) and GSLE soundings (red). Black dashed line indicates the 16°C operational forecast threshold, and red dashed line the quadratic curve fit for a seasonally varying threshold (ΔT_{min}). Blue line denotes climatological lake temperature.

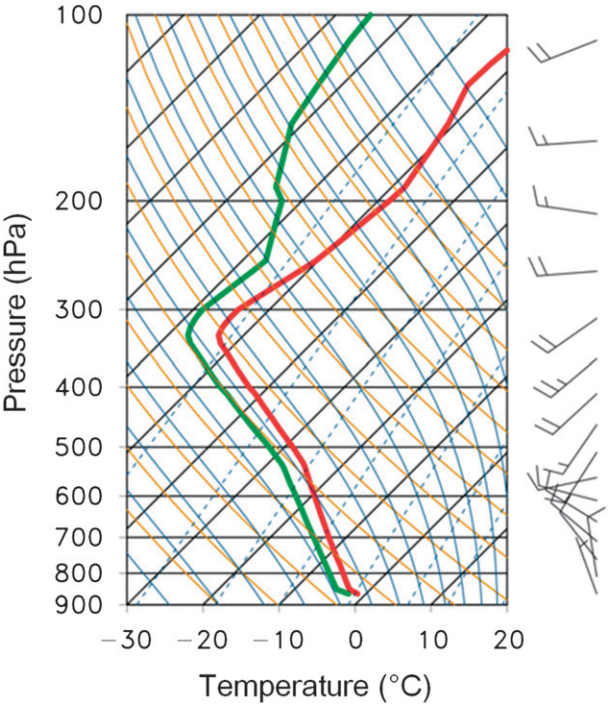

FIG. 7. Skew T–log$p$ [temperature, dewpoint, and wind barbs (full and half barbs denote 5 and 2.5 m s^{-1}, respectively)] diagram for KSLC at 1200 UTC 2 Jan 2000.

and in early April (Fig. 6a). Our results differ from those of Steenburgh et al. (2000), who found a midwinter peak in event frequency for 1994–98. This discrepancy might reflect the smaller sample size (34 events versus 149 in the current study), differing techniques for event identification, and/or missing radar data shortly after KMTX became operational in 1994.

b. Factors affecting the occurrence of GSLE

1) LAKE–ATMOSPHERE TEMPERATURE DIFFERENCE

The mean lake–700-hPa temperature difference (ΔT) for GSLE events is 20.7°C, but in 9 of the 143 GSLE soundings ΔT was less than 16°C, with these occurrences confined to 4 December– 12 February. This finding indicates that ΔT corresponding to a dry-adiabatic lapse rate (e.g., Holroyd 1971; Niziol 1987; Carpenter 1993; Niziol et al. 1995; Steenburgh et al. 2000) is not an absolute minimum for the occurrence of GSLE, which calls into question the use of this threshold in operational forecasting. On 5 January 2007, GSLE produced snowfall totals of 10–20 cm in the Salt Lake and Tooele Valleys with a ΔT of only 14.1°C. The lowest ΔT associated with GSLE in this study was 12.4°C at 1200 UTC 2 January 2000, when the sounding exhibited a moist-adiabatic lapse rate and near-saturated conditions up to the tropopause (Fig. 7). High values of ΔT were reached much less often during winter due to a lake temperature remaining near 0°C, a result that may partially explain the winter minimum in event frequency.

Although low ΔT (<16°C) values could arise from errors in the regression estimation of lake temperature, the mean absolute error in lake temperature estimation during December–February was only 0.9°C, so this contribution is expected to be small. Alternatively, events featuring low ΔT values could be due to the erroneous attribution of precipitation features to lake-effect processes. A reexamination of the radar data for these events suggests that this source of error is unlikely. Parcel theory suggests that when the boundary layer profile is saturated and moist adiabatic, any ΔT greater than a moist-adiabatic lapse rate could be sufficient for

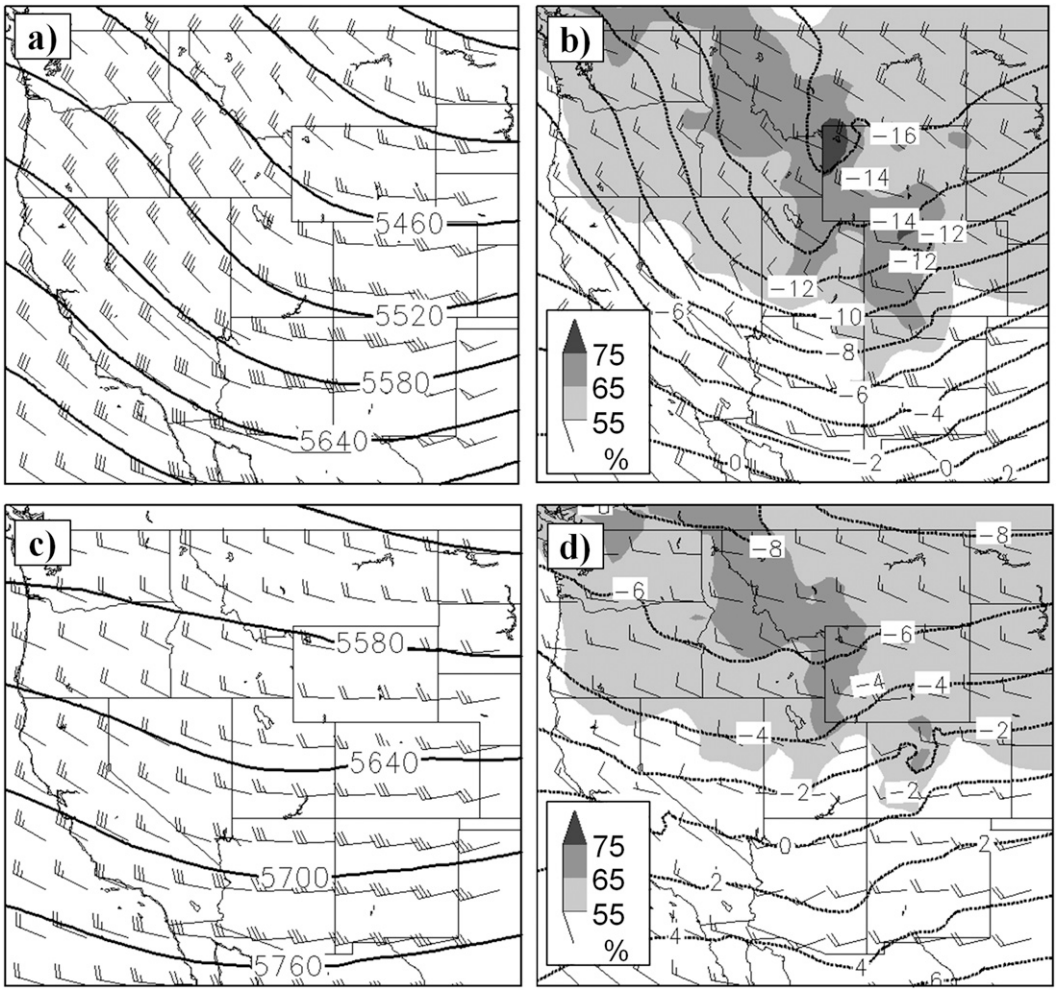

FIG. 8. NARR composite (a) 500-hPa geopotential height (solid contours) and 500-hPa wind (full and half barbs denote 5 and 2.5 m s^{-1}, respectively); (b) 700-hPa temperature (dashed contours, °C), 700-hPa wind, and 850–700-hPa mean layer RH (%, shaded according to scale at left), for winter (December–February) soundings with $16° < \Delta T < 19°C$. (c),(d) As in (a),(b), but for fall and spring (September–November, March–May) soundings.

overlake flow to yield a buoyant surface parcel. For 700-hPa temperatures of −20° and 0°C, this lapse rate would be achieved at ΔT of 13° and 10°C, respectively.

The monthly minimum ΔT associated with GSLE (hereafter ΔT_{min}) exhibits a marked seasonal variation, decreasing from 21°C in September to 12°C in January, and increasing again to 22°C in May (Fig. 6b). While occasionally observed in winter when ΔT was from 12° to 18°C, GSLE only occurred in April–May when ΔT exceeded 19°C. Long nights and widespread snow cover in winter may be more favorable for persistent land-breeze circulations and overlake convergence, which could contribute to the development of GSLE with relatively low values of ΔT. However, the mean lake–land temperature difference is in fact smaller during winter GSLE events, and the seasonal dependence of ΔT_{min} more likely reflects the climatological relationship between ΔT and the synoptic environment.

In winter, ΔT rarely reaches as high as the 16°–19°C range, but the composite NARR analysis for all winter soundings (with or without GSLE) when $16° \leq \Delta T \leq 19°C$ shows a 500-hPa trough, 700-hPa flow from the northwest, and high low-level relative humidity in the GSL region—all conditions that Steenburgh et al. (2000) indicate are favorable for GSLE (Figs. 8a,b). During April–May, ΔT exceeds 16°C in 41% of all soundings, but the composite analysis for all soundings with $16° \leq \Delta T \leq 19°C$ in April–May shows near zonal flow at 500 and 700 hPa, and drier air at low levels (Figs. 8c,d). Thus, while values of ΔT considered marginally sufficient for

GSLE occur very frequently in the warmer months, these values were often accompanied by high environmental stability, unfavorable flow, and inadequate low-level moisture.

Fitting a quadratic curve to the monthly minimum ΔT points ($\Delta T_{\min}$) is a simple approach to developing a seasonally varying threshold as an alternative to a single value (e.g., 16°C). The equation for this best fit curve (plotted in Fig. 6b) is

$$\Delta T_{\min} = 0.000\,642\,5d^2 - 0.152d + 21.35(^{\circ}\mathrm{C}),$$

where d is the number of days since 15 September. The remainder of the manuscript will refer to $\Delta T - \Delta T_{\min}$ as the excess of ΔT (hereafter ΔT_{excess}) in a given sounding above this seasonally varying threshold. By this method, $\Delta T_{\text{excess}} \geq 0$°C is considered the minimum "requirement" for GSLE, although some values associated with GSLE are slightly less than zero due to an imperfect $\Delta T_{\min}$ curve fit.

Figure 9 shows ΔT_{excess} values for four types of soundings: (a) soundings with no lake effect, (b) soundings with a lake effect, (c) soundings with a pure lake effect (i.e., when no transient or non-lake-effect precipitation is present) and a low coverage of radar echoes ≥10 dBZ (<80 km^2, the lowest tertile of this parameter), and (d) soundings with a pure lake effect and a high coverage of radar echoes ≥10 dBZ (>600 km^2, the highest tertile). The median value of ΔT_{excess} for all soundings with GSLE was 4.0°C, with a maximum of 11.4°C. Large values of ΔT_{excess} do not indicate an increased likelihood of high-coverage events, and in fact the median ΔT_{excess} for high-coverage events (3.4°C) is significantly lower than for low-coverage events (5.5°C).

When considering only ΔT_{excess}, there remains a large portion of soundings where the seasonally varying threshold is exceeded but no lake effect occurs. In fact, no GSLE was observed within 12 h for 77% of soundings with $\Delta T_{\text{excess}} \geq 0$°C, a result that necessitates the examination of additional environmental variables.

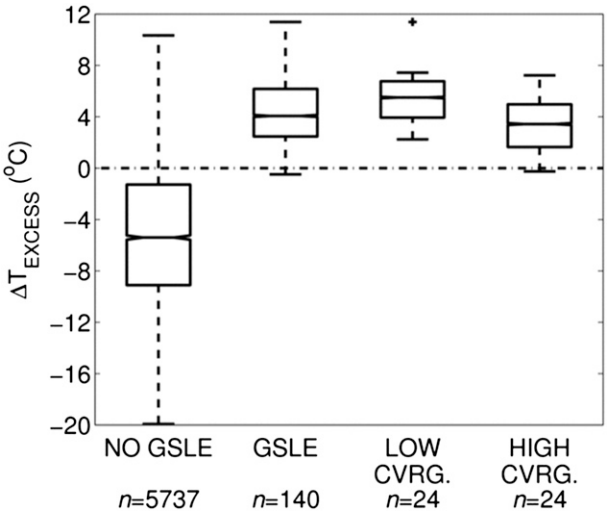

FIG. 9. Comparison of ΔT_{excess} for four categories of soundings: soundings with GSLE, without GSLE, with a pure lake effect and low coverage (<80 km^2 of 10-dBZ radar echoes, the lowest tertile), and with a pure lake effect and high coverage (>640 km^2 of 10-dBZ radar echoes, the highest tertile). Box top and bottom are the 25th and 75th percentiles, the median is denoted by a horizontal line in the box (medians of two distributions differ at the 90% level when the notches around their respective median lines do not overlap), whiskers extend to 1.5 times the interquartile range, and outliers beyond 1.5 times the interquartile range are denoted by plus signs (+).

2) ENVIRONMENTAL MOISTURE

The presence of low-level moisture is crucial for GSLE events, and low relative humidity values may preclude the development of lake-effect precipitation even when ΔT_{excess} is large. Among moisture variables, the largest difference in the medians for GSLE and non-GSLE soundings, given $\Delta T_{\text{excess}} \geq 0$°C, was found for 850–700-hPa layer-mean relative humidity ($RH_{850–700}$), and the median $RH_{850–700}$ for GSLE soundings (81%) was considerably higher than for non-GSLE soundings (67%) (Fig. 10a). High-coverage GSLE soundings exhibited a slightly higher median $RH_{850–700}$ than did low-coverage soundings (83% versus 77%, respectively; significant at the 90% level). There were no GSLE soundings with a $RH_{850–700} < 53\%$ and no high-coverage GSLE soundings with a $RH_{850–700} < 60\%$. Only 27% of soundings with a $\Delta T_{\text{excess}} \geq 8$°C and a $RH_{850–700} < 60\%$ were associated with GSLE, versus 72% for a $\Delta T_{\text{excess}} \geq 8$°C and a $RH_{850–700} \geq 60\%$ (not shown), indicating that a large value of ΔT_{excess} was often insufficient for GSLE when dry air was present at low levels.

The median values of midlevel (700–500-hPa) layer-mean relative humidity ($RH_{700–500}$; Fig. 10b) were also significantly higher for GSLE (71%) than for non-GSLE soundings (56%). However, several GSLE soundings had $RH_{700–500}$ less than 30%, perhaps reflecting the existence of GSLE convection primarily in the lowest 1–3 km above ground. Soundings with high-coverage GSLE showed very high median $RH_{700–500}$ relative to low-coverage soundings, with a median of 76% and no values less than 55%. Occurrences of high-coverage GSLE therefore tend to depend on the presence of both low- and midlevel moisture.

The importance of moisture for lake-effect precipitation is underscored by past research. Steenburgh et al. (2000) found no GSLE events with a 700-hPa relative humidity less than 54%, and Kristovich and Laird

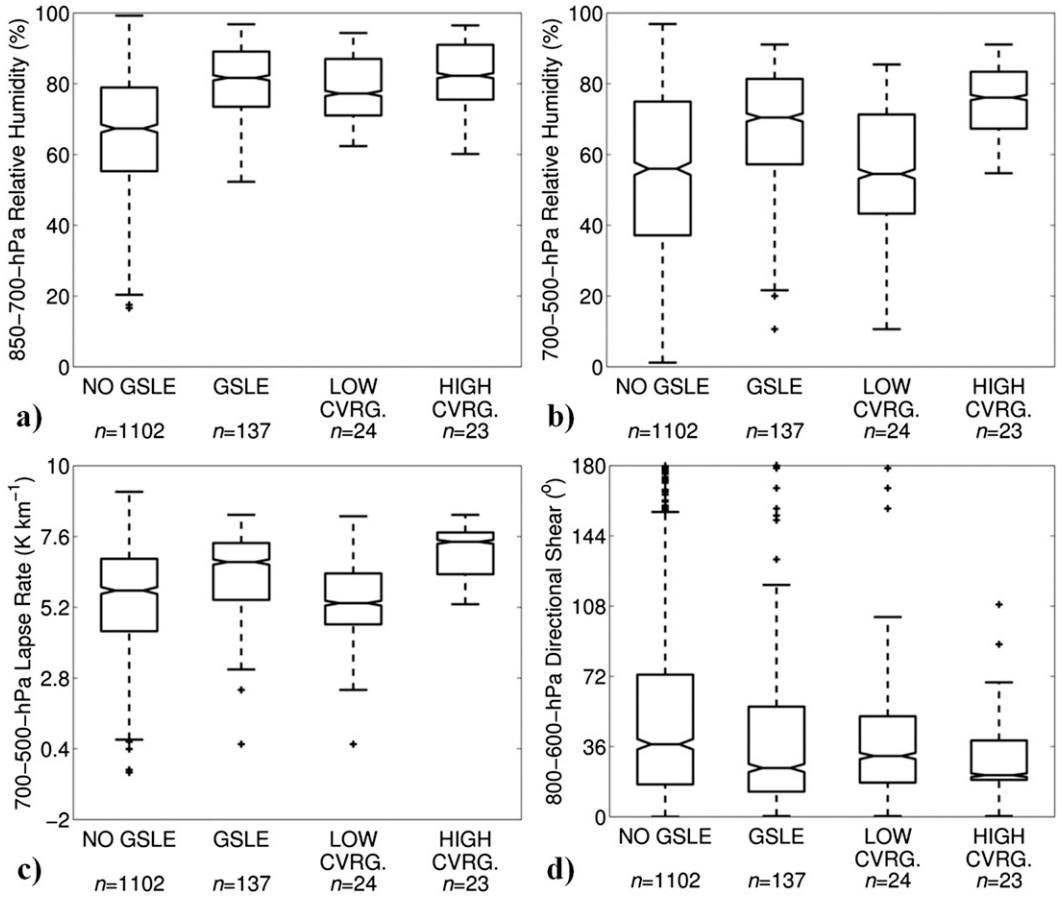

FIG. 10. Comparison of variables in the same categories of soundings as in Fig. 9, but for $\Delta T_{\text{excess}} \geq 0$: (a) 850–700-hPa mean layer RH (%), (b) 700–500-hPa mean layer RH (%), (c) 700–500-hPa lapse rate (K km^{-1}), and (d) 800–600-hPa directional shear (°). Box-and-whiskers plotting convention as in Fig. 9.

(1998) highlight the dependence of lake-effect cloud formation on upstream moisture conditions, suggesting that moisture might play a key role in determining whether GSLE convection develops. Around the Great Lakes, where upstream moisture is perhaps less important due to longer overlake fetch, neither Niziol (1987) nor Niziol et al. (1995) include relative humidity when describing significant parameters in the operational forecast process for lake-effect snow.

3) STABILITY AND WIND SHEAR

The median 700–500-hPa lapse late for GSLE was 6.7 K km^{-1}, significantly greater than that of non-GSLE soundings (5.7 K km^{-1}; Fig. 10c), suggesting that mid-level environmental stability is also important for the occurrence of GSLE, given the presence of sufficient ΔT_{excess}. The median 700–500-hPa lapse late for high-coverage events (7.3 K km^{-1}) greatly exceeded the median for low-coverage events (5.3 K km^{-1}), indicating a tendency for more widespread precipitation to occur when conditional instability is present at midlevels.

Soundings with GSLE were associated with lower median values of 800–600-hPa[1] directional shear than were non-GSLE soundings (25° versus 37°, respectively; Fig. 10d). The median value for high-coverage events (21°) was also significantly lower than for low-coverage events (31°). However, high values of directional shear (>60°) alone did not decrease the likelihood of GSLE, given that modest lake-induced instability and low-level moisture were present. For $\Delta T_{\text{excess}} \geq 4$°C and $\text{RH}_{850-700} \geq 60\%$, GSLE was associated with 32% of soundings with 800–600-hPa directional shear ≤ 60°, and 30% of soundings with directional shear > 60° (not shown). In fact, there were eight soundings where GSLE was associated with directional shear ≥ 90° and 700-hPa wind speeds > 5 m s^{-1}, including one high-coverage event. These results conflict with findings in previous studies. Niziol (1987) found from discussions

[1] This layer was chosen following Steenburgh et al. (2000), who describe it as the ''steering layer.''

with forecasters that low-level (surface–700 hPa) wind shear greater than 60° tended to prevent lake-effect convection on the Great Lakes. Steenburgh et al. (2000), who studied a much smaller sample of GSLE events, found only one radiosonde observation during a GSLE event where 800–600-hPa directional shear exceeded 60°.

4. Wind direction

The median wind direction in GSLE soundings was 315° at 700 hPa, and 325° at 800 hPa, with the latter value corresponding to the direction of maximum fetch over the GSL. The GSL has a large horizontal aspect ratio, and fetch is dramatically reduced for wind directions approaching the southwest or northeast, from a peak of ~125 km at 325° and 145° down to ~40 km at 235° and 55°. Accordingly, for $\Delta T_{\text{excess}} \geq 0$ and $\text{RH}_{850\text{–}700} \geq 55\%$, 22% of soundings with 700-hPa wind directions between 292° and 7° were associated with GSLE, versus only 9% with winds outside this range (Fig. 11). In all of the soundings examined by Steenburgh et al. (2000), the 700-hPa wind direction was between 285° and 5°, but our analysis of a larger sample of radar data found that the 700-hPa wind direction was outside of this range in 16% of soundings associated with GSLE. While at some of these sounding times weak GSLE convection was present in unusual areas [e.g., the far northern Wasatch Front, Skull Valley, and the West Desert region (see Fig. 1 for locations)], wind speeds were otherwise very light (<3 m s^{-1}) and lower-level flow (i.e., at 800 hPa) was still from the west, northwest, or north.

5. Lake–land temperature difference

The timing of GSLE events suggests the importance of land-breeze convergence for convective initiation. There was a strong tendency for GSLE to initiate in the overnight hours and end during the day, a characteristic shared by 73% of events. The median start time for events was 3.1 h after sunset (Fig. 12a), and the median end time was 2.7 h after sunrise (Fig. 12b). Only 12 events (8%) initiated between noon and sunset. GSLE was most likely to be present between 1100 and 1500 UTC [0400–0800 local standard time (LST)], and least likely between 2100 and 0100 UTC (1400–1800 LST; Fig. 12c), times that correspond, respectively, to the maximum and minimum values of lake–land temperature difference[2] ($\Delta T_{\text{LAKE–LAND}}$).

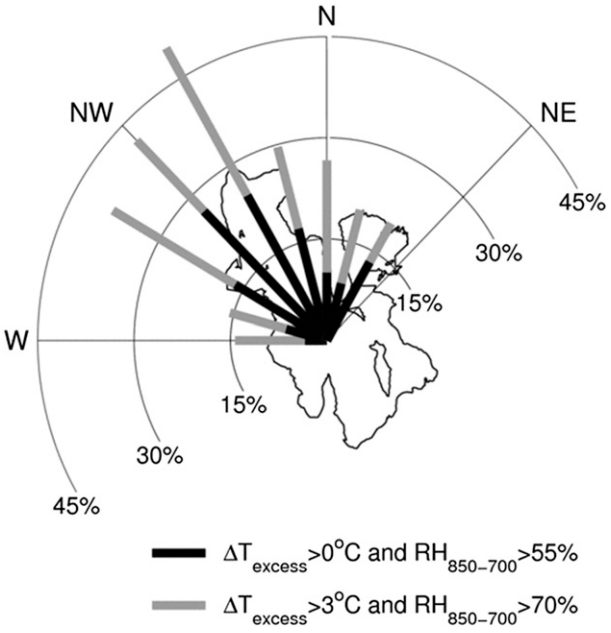

FIG. 11. Fraction of soundings (%) with GSLE vs 700-hPa wind direction, overlaid on GSL shoreline map, given $\Delta T_{\text{excess}} \geq 0$ and $\text{RH}_{850\text{–}700} \geq 55\%$ (black bars) or $\Delta T_{\text{excess}} \geq 3$ and $\text{RH}_{850\text{–}700} \geq 70\%$ (gray bars).

On days with GSLE, the median values of $\Delta T_{\text{LAKE–LAND}}$ were 7.8°, 4.5°, and 6.1°C at midafternoon, and 12.2°, 8.3°, and 11.7°C in the early morning, during the fall, winter, and spring, respectively (Fig. 12d). The maxima in $\Delta T_{\text{LAKE–LAND}}$ clearly correspond with the times of peak GSLE frequency (i.e., Fig. 12c). There were no times over the entire period of record where GSLE occurred with a lake temperature colder than the mean temperature at adjacent land stations (i.e., $\Delta T_{\text{LAKE–LAND}} < 0$). On a lake that is warmer than the adjacent land surface, a confluence zone and surface pressure trough may develop where offshore flow from one side of a lake opposes either the mean flow or offshore flow from the other side (e.g., Hjelmfelt 1990). When instability is sufficient, convective updrafts in this confluence zone strengthen the incoming land breezes and effectively generate a ''self-maintaining'' system (Passarelli and Braham 1981). The concept of land breezes driving convective initiation brings forth difficulty in the determination of cause and effect, in that convective structures may induce their own local wind field. However, the large magnitude of $\Delta T_{\text{LAKE–LAND}}$ on days with GSLE, and the timing of events, suggest that mesoscale thermally driven flows are likely to play a significant role in initiating and maintaining GSLE.

The diurnal modulation of GSLE exhibits marked seasonal differences that appear counterintuitive within the context of thermally driven circulations. Several

[2] The lake–land temperature difference ($\Delta T_{\text{LAKE–LAND}}$) is computed as the difference between the GSL temperature and the mean 2-m temperature at 11 mesonet sites surrounding the GSL (see Fig. 1 for locations). Positive values of $\Delta T_{\text{LAKE–LAND}}$ indicate that the GSL is warmer than land stations.

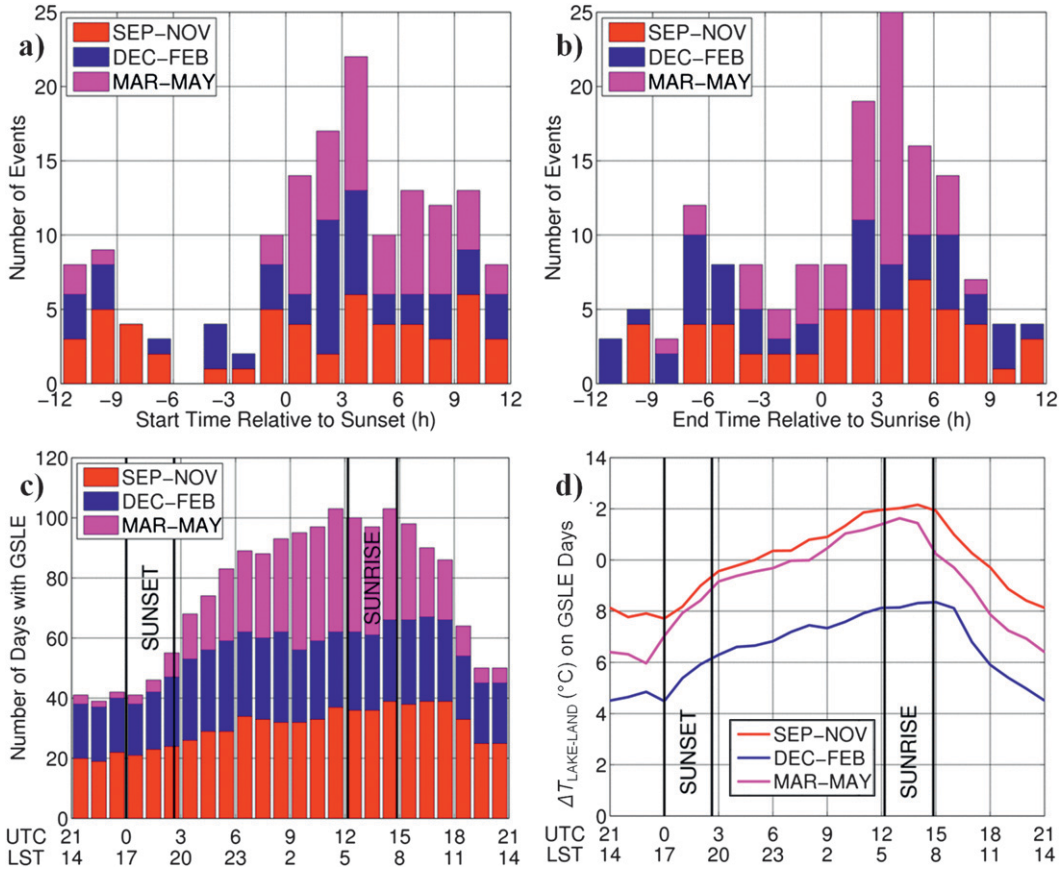

FIG. 12. Timing of GSLE events: (a) event start time relative to sunset (h); (b) event end time relative to sunrise (h); (c) number of days with GSLE at a given time of day (h, UTC and LST), where vertical bars indicate the ranges of sunrise and sunset times (16 September–15 May); and d) hourly median $\Delta T_{\text{LAKE–LAND}}$ on days with GSLE.

GSLE events persist throughout the day in fall, and the frequency of GSLE in winter has almost no dependence on time of day. However, GSLE is very rare in spring between 1900 and 0200 UTC (1200–1900 LST), despite median $\Delta T_{\text{LAKE–LAND}}$ values that are comparable to or greater than those in the fall. Analysis of radar imagery reveals a tendency for events in spring to transition to disorganized land-based convection during the afternoon, despite atmospheric profiles favorable for GSLE. Conversely, winter events often retain organized lake-effect convection through the afternoon hours with much lower values of $\Delta T_{\text{LAKE–LAND}}$. We attribute this seasonal contrast to the presence of more intense daytime surface heating in spring, when the solar zenith angle is smaller, which yields deeper mixing and drier air at low levels by midafternoon. On days with GSLE, 1200 UTC (0500 LST) profiles of median relative humidity were similar in fall, winter, and spring (Fig. 13). At 0000 UTC (1700 LST), however, the median relative humidity in the lowest levels (i.e., 850–800 hPa) dropped to 40%–50% in spring, versus 60% in fall and winter. Several studies point to decreasing upstream low-level relative humidity due to afternoon turbulent mixing as a mechanism for the diurnal modulation of lake-effect precipitation (e.g., Lavoie 1972; Hjelmfelt 1990; Kristovich and Spinar 2005). Although the KSLC sounding site is generally downstream of the GSL in the majority of GSLE events, the observed daytime drying at low levels is likely to be occurring throughout the surrounding region, thus removing the crucial moisture ingredient necessary for lake-effect precipitation.

c. GSLE morphology

GSLE precipitation covers a wide range of convective modes, from widespread areas of nonbanded structures to narrow, solitary bands. We found nonbanded precipitation was the most frequently observed mode, comprising 54% of the 605 analyzed 3-h GSLE periods. The remaining periods were characterized as either mixed mode (25%; primarily nonbanded with some embedded linear features), or banded (20%). Banded periods were

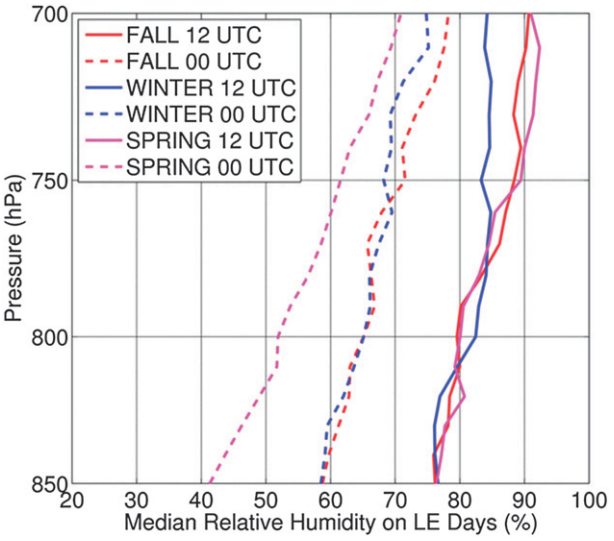

FIG. 13. Profiles of median RH (%) on days with GSLE.

less common in the winter months (December–February), comprising only 10% of GSLE periods, than in fall (27%) or spring (25%). Steenburgh et al. (2000) suggested a link between midlake banded structures and the existence of thermally driven convergence, and accordingly we found a significant increase in the frequency of banded GSLE when $\Delta T_{\text{LAKE–LAND}}$ was large. For $\Delta T_{\text{LAKE–LAND}} < 4°\text{C}$, only 13% of GSLE periods were banded, versus 30% for $\Delta T_{\text{LAKE–LAND}} > 14°\text{C}$.

The morphology differentiation factor U/L (wind speed divided by fetch) proposed by Laird et al. (2003b) in the Great Lakes shows some utility for GSLE, although the classification scheme in the current study differs considerably from the one used in the Great Lakes. Values of U/L were calculated using the 800-hPa wind speed, the level at which the relationship between U/L and GSLE mode was found to be strongest. High values of U/L (i.e., >0.08 m s^{-1} km^{-1}) are associated with banded GSLE (Fig. 14a), features that are similar in structure to midlake and shoreline bands observed over the Great Lakes. High values of U/L in the Great Lakes instead tend to favor widespread coverage events. Low values of U/L in the Great Lakes (i.e., <0.05 m s^{-1} km^{-1}) are typical of mesoscale vortex events, but only one GSLE period showed any signs of an organized circulation (not shown). There exists, however, substantial overlap in the conditions associated with nonbanded and banded periods, indicating that the relationship between U/L and GSLE mode is weak.

Banded convection in the boundary layer is generally associated with stronger low-level winds and speed shear than nonlinear or cellular convection (Kristovich 1993; Kristovich et al. 1999; Weckwerth et al. 1997).

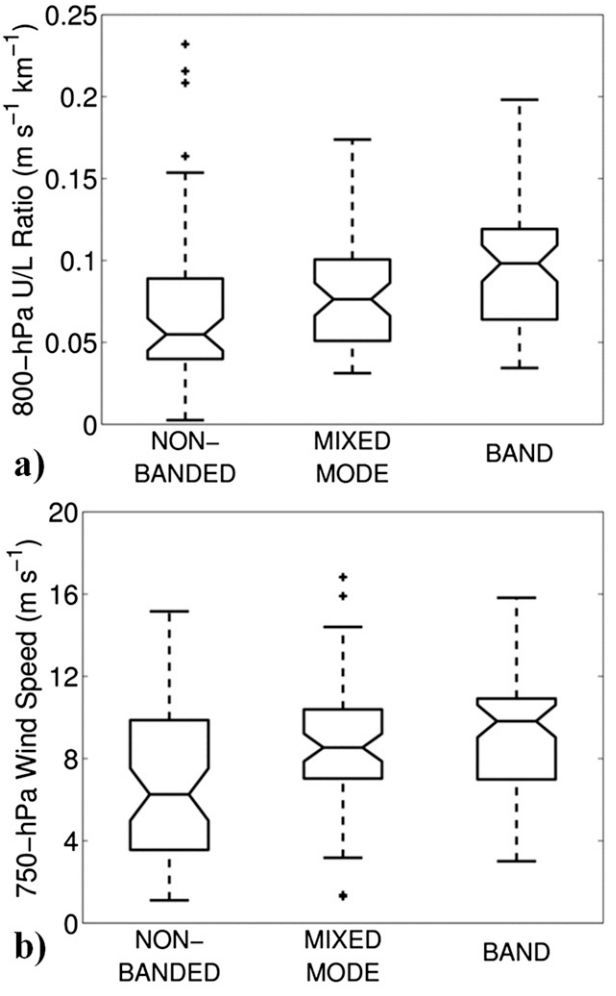

FIG. 14. GSLE mode vs (a) 800-hPa wind speed–fetch ratio (U/L; m s^{-1} km^{-1}), and (b) 750-hPa wind speed (m s^{-1}). Box-and-whiskers plotting convention as in Fig. 9.

Model sensitivity studies of a Great Lakes lake-effect event by Cooper et al. (2000) showed a shift from horizontal rolls to cellular convection when boundary layer wind speeds were reduced below 5 m s^{-1}, while variations in the thermodynamic profile had little impact on convective mode. Similarly, banded periods in this study occurred with significantly stronger 750-hPa wind speeds than did nonbanded structures (Fig. 14b; the level at which this relationship was strongest). The median speed shear in the lowest 100 hPa was also slightly higher for banded GSLE, but the difference was not significant at the 90% level. The relationship between GSLE morphology and lake-induced or environmental instability was weak, but banded GSLE tended to occur with slightly greater values of ΔT and low-level lapse rate (not shown). Overall, the environmental conditions associated with nonbanded versus banded GSLE

TABLE 3. Utility of various forecast parameters, where $N_{soundings}$ is the total number of soundings that meet the given criteria, N_{GSLE} is the number of soundings that meet the criteria and are associated with GSLE, FO is the frequency of occurrence of GSLE, FAR is the false alarm rate, and POD is the probability of detection.

Condition	$N_{soundings}$	N_{GSLE}	FO (%)	FAR (%)	POD (%)
$\Delta T \geq 16$°C	1432	275	19	81	91
$\Delta T \geq 22$°C	365	120	33	67	47
$\Delta T \geq 25$°C	38	19	50	50	12
$\Delta T \geq 16$°C and shear < 60°	936	194	21	79	72
$\Delta T \geq 16$°C, shear < 60°, and no stable layers	619	145	23	77	55
$\Delta T_{excess} \geq 0$	1134	264	23	77	96
$\Delta T_{excess} \geq 2$	673	203	30	70	79
$\Delta T_{excess} \geq 0$ and $RH_{850–700} > 55\%$	884	236	27	73	94
$\Delta T_{excess} \geq 2$ and $RH_{850–700} > 55\%$	529	189	36	64	79

convection exhibit only minor differences, but there is some tendency for banded GSLE to dominate when U/L is high, low-level wind speeds are strong, and $\Delta T_{LAKE–LAND}$ is large.

4. Implications for operational weather forecasting

Operational forecasting of GSLE currently involves identifying periods of west–north flow at 700 hPa and a lake–700-hPa temperature difference (ΔT) exceeding 16°C, with minimal consideration of low-level moisture (L. Dunn, National Weather Service, 2011, personal communication). This existing forecasting methodology rarely results in a missed event (i.e., a high probability of detection), but yields a high false alarm rate. Of 881 soundings with $\Delta T \geq 16$°C and a 700-hPa wind direction between 270° and 360°, only 200 (22%) were associated with GSLE within 12 h, a fairly generous verification window (Table 3). Although much more likely at high values of ΔT (i.e., ≥22°C), GSLE was still only associated with 38% of soundings satisfying this condition. Consideration of other parameters (e.g., weak 800–600-hPa directional shear and the absence of stable layers or temperature inversions in the lowest 150 hPa) suggested by Steenburgh et al. (2000) leads to some improvement, but the false alarm rate remains high (Table 3).

Based on our revised climatology, the use of a seasonally varying ΔT threshold reduces the number of these false alarms due to a higher threshold in the early fall and spring. Further improvement results from including an $RH_{850–700}$ threshold of 55%. Nonetheless, forecasting of GSLE or other relatively rare events (such as tornadic thunderstorms) is often limited by the use of exclusively deterministic techniques such as the exceedance of specific thresholds (e.g., Murphy 1991).

We propose a probabilistic forecast methodology for GSLE that considers ΔT_{excess}, $RH_{850–700}$, and 700-hPa wind direction. Figure 15a shows the fraction of soundings associated with GSLE for ranges of both ΔT_{excess} and $RH_{850–700}$, regardless of 700-hPa wind direction, calculated over intervals of 1°C and 8%, respectively. Given a good forecast of the environmental conditions, and a lake temperature calculated using the approach described in section 2, Fig. 15a translates to the probability of GSLE. Thus, the probability of GSLE increases with increasing ΔT_{excess} and $RH_{850–700}$, and exceeds 80% for $\Delta T_{excess} \geq 8$°C and $RH_{850–700} \geq 90\%$. Plots for 290°–360° and 1°–289° 700-hPa wind directions are shown in Figs. 15b and 15c, respectively, indicating higher probabilities of GSLE in 290°–360° flow than for other wind directions, regardless of the magnitudes of ΔT_{excess} and $RH_{850–700}$.

One difficulty in forecasting the occurrence of GSLE by the aforementioned probabilistic method stems from uncertainty in operational model forecasts of low-level relative humidity and 700-hPa temperature. North American Mesoscale Model (NAM) forecasts for KSLC on days when GSLE was possible ($\Delta T_{excess} \geq 0$ at 0000 or 1200 UTC) were skewed to higher values of $RH_{850–700}$ (Fig. 16), and slightly warmer values of 700-hPa temperature (not shown) relative to observed raob soundings. The mean bias in these 24-h forecasts of $RH_{850–700}$ and 700-hPa temperature were 10% and 0.7°C, respectively. Absolute errors in $RH_{850–700}$ averaged 12% and exceeded 25% in several cases. Absolute errors in 700-hPa temperature were small however, and averaged only 1.1°C. Assuming NAM biases have not changed, these results suggest that direct application of Fig. 15 (utilizing NAM output) in operations could overestimate the probability of GSLE.

Another forecast concern is the GSL temperature estimate. In general, the GSL temperature can be reliably estimated from recent MODIS data, but long periods of mostly cloudy to overcast conditions preclude the retrieval of recent temperature data and provide an additional source of error in calculating ΔT_{excess}. When MODIS data are unavailable or unreliable, forecasters can employ the technique for

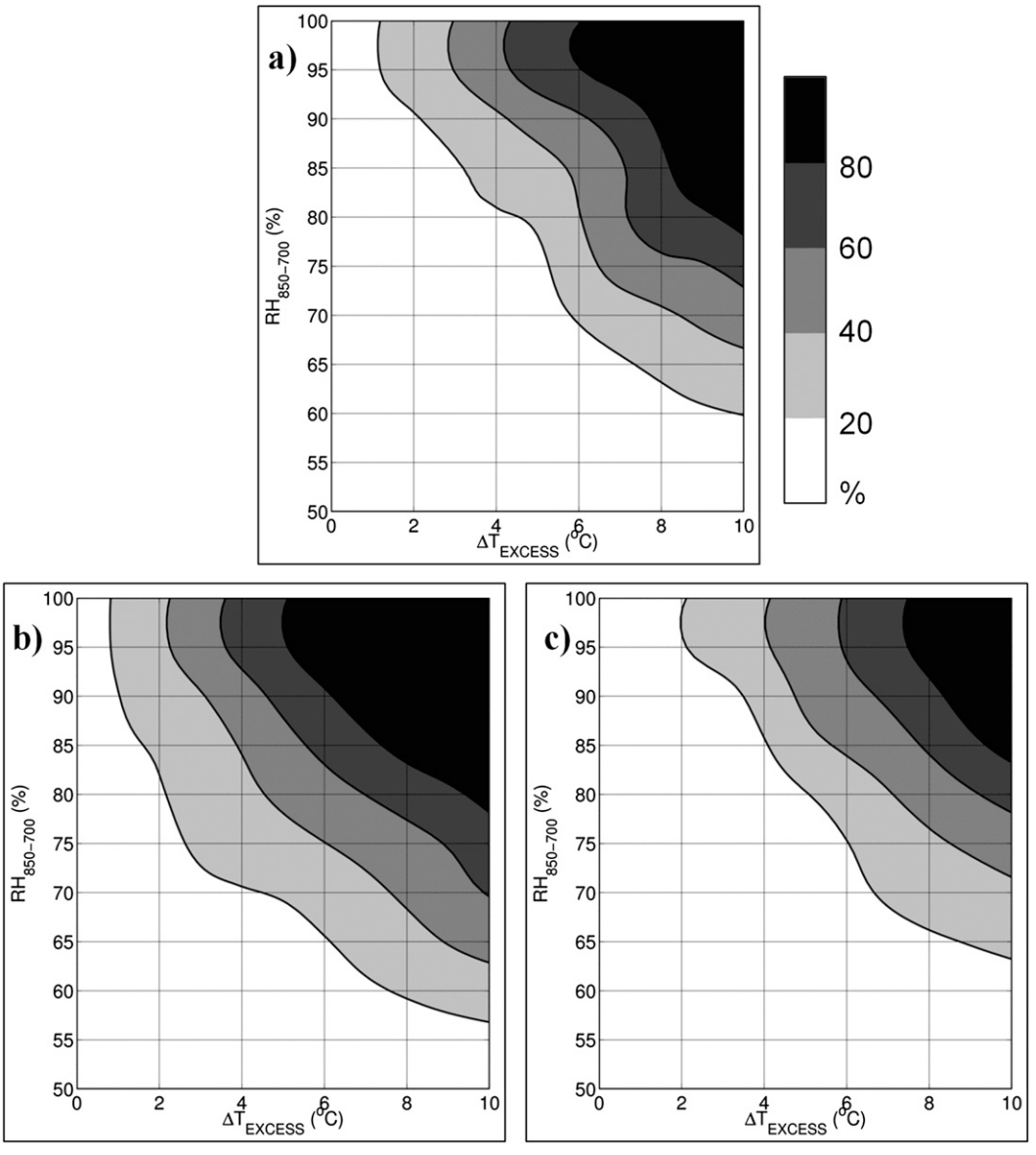

FIG. 15. (a) Fraction of soundings with GSLE (%, shaded according to scale at right) as a function of ΔT_{excess} (°C) and $RH_{850–700}$ (%). (b) As in (a), but for 700-hPa wind directions 290°–360°. (c) As in (a), but for 700-hPa wind directions 1°–289°.

estimating GSL temperature described in section 2 of this paper, acknowledging that errors can occasionally exceed 2°C.

The relationship between ΔT and the coverage of GSLE was weak, and our results alternatively suggest considering 700–500-hPa lapse rate and $RH_{700–500}$. Although low-coverage (<80 km^2) GSLE can occur even at high values of both variables, major GSLE (>640 km^2) occurred almost exclusively with a 700–500-hPa lapse rate ≥ 5.5 K km^{-1} and $RH_{700–500} \geq 60\%$ (Fig. 17). Given that GSLE is expected, values outside of this phase space can indicate to forecasters that the areal coverage of precipitation is likely to be low.

5. Conclusions

Radar data were examined over a 13-yr period to identify 149 GSLE events affecting northern Utah. Large interannual variability exists in event frequency, and is more strongly correlated with atmospheric factors than the area of the GSL. GSLE events exhibited fall and spring peaks in frequency, and were less common in

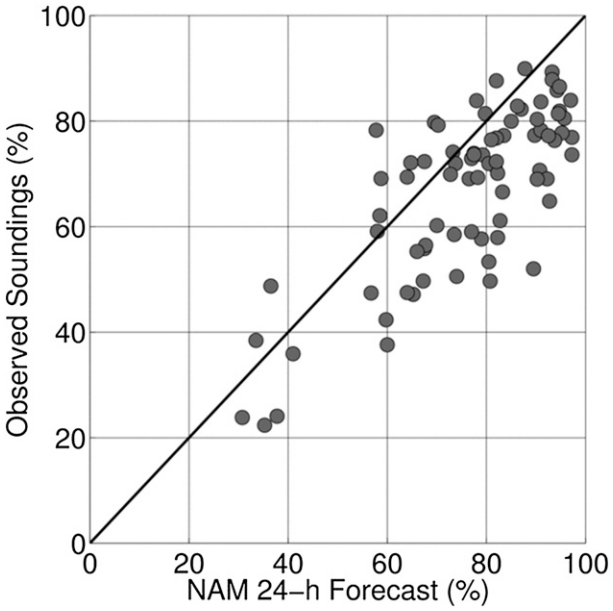

FIG. 16. Observed 850–700-hPa RH (%) from KSLC soundings vs 24-h NAM forecasts, from the 2008/09 and 2009/10 cool seasons. Diagonal line indicates a perfect forecast.

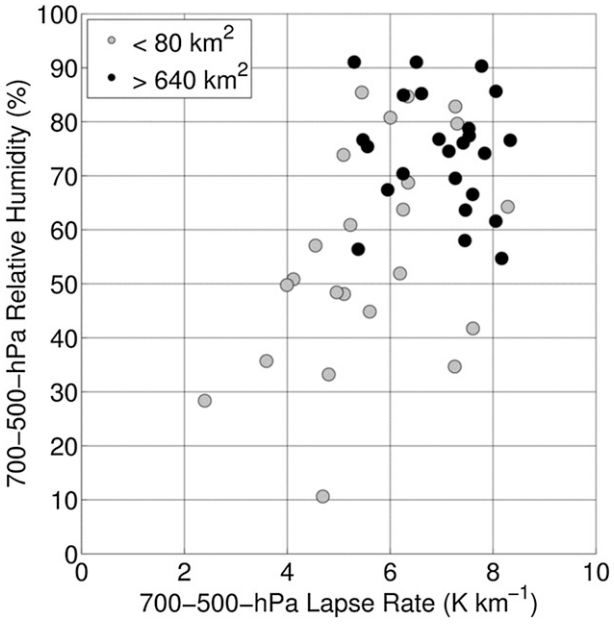

FIG. 17. GSLE coverage (area extent of radar echoes ≥10 dBZ; km^2) vs 700–500-hPa lapse rate and RH.

midwinter when the lake temperature fell to near freezing. In the coldest months, GSLE occurred at values of lake–700-hPa temperature difference (ΔT) less than the 16°C (Steenburgh et al. 2000) or 17°C (Carpenter 1993) thresholds often used in operational forecasting. In fall and spring, however, GSLE occurs only at much higher values of ΔT. A seasonally varying threshold (ΔT_{min}), calculated from a quadratic curve fit to the monthly minimum ΔT values for GSLE soundings, is considered more appropriate for use in forecast applications than a single threshold value. The minimum requirement for GSLE is thus a positive value of ΔT_{excess}, equal to $\Delta T - \Delta T_{\text{min}}$.

A large positive ΔT_{excess} does not guarantee that GSLE convection will initiate, and our results suggest that low-level moisture is a crucial secondary ingredient. Higher relative humidity and steeper lapse rates at midlevels, while not crucial for GSLE development, are associated with high-coverage events. Alignment of the 700-hPa flow along the long axis of the GSL (i.e., near 325°) also substantially increases the likelihood of a lake effect above that observed with westerly or northeasterly flow. GSLE only occurred when the lake temperature was greater than the average temperature at adjacent land stations, suggesting the importance of thermally driven land breezes in the initiation and maintenance of convection. Finally, large values of low-level directional shear were not found to inhibit GSLE formation when thermodynamic profiles were otherwise favorable.

Banded GSLE, which tends to be associated with higher snowfall rates and thus greater transportation impacts, was more common than widespread, nonbanded convection when low-level (750 hPa) winds were strong (>7 m s^{-1}) and when the lake temperature was much warmer than adjacent land stations. However, it remains an issue that there is substantial overlap in the conditions associated with these GSLE modes. Sensitivity to low-level moisture and wind direction, and vague distinctions between morphological parameter spaces perpetuate the difficulties of forecasting the occurrence and mode of these storms.

Based on these results, we propose a probabilistic approach to forecasting the occurrence of GSLE that considers ΔT_{excess}, 850–700-hPa relative humidity, and 700-hPa wind direction (see Fig. 15). Although not a perfect indicator, the 700–500-hPa lapse rate and 700–500-hPa relative humidity can be used to anticipate the areal coverage of GSLE precipitation. This methodology has the potential to reduce false alarms encountered with the existing techniques, particularly through consideration of low-level moisture and a seasonally varying threshold for ΔT. The National Weather Service in Salt Lake City has recently incorporated findings from this study into their operations. Forecast errors in current 12-km operational NAM (and other) model guidance provide an additional source of uncertainty, and could lead forecasters to overestimate (in the case of the NAM) the probability of GSLE. Nonetheless,

implementation of the new probabilistic method offers the potential for improved prediction of events that can have significant transportation impacts along the Wasatch Front urban corridor.

Acknowledgments. We thank the summer 2007 undergraduate students at Hobart and William Smith Colleges, Benjamin Albright and Jessica Popp, who performed the initial event identification, and Meteorologist-in-Charge Larry Dunn and Science Operations Officer Randy Graham of the National Weather Service Forecast Office in Salt Lake City for their guidance and perspectives in the operational forecasting realm. We gratefully acknowledge the provision of datasets, software, and/or computer time and services provided by NCDC, NCEP, NCAR, Unidata, the University of Wyoming, and the University of Utah Center for High Performance Computing. Comments from three anonymous reviewers improved the manuscript. This research is based in part on work supported by a series of grants provided by the NOAA/National Weather Service CSTAR program and Grant AGS-0938611 from the National Science Foundation. Any opinions, findings, and conclusions or recommendations expressed in this material are those of the authors and do not necessarily reflect those of the National Science Foundation or the National Weather Service.

REFERENCES

Braham, R. R., and M. J. Dungey, 1984: Quantitative estimates of the effect of Lake Michigan on snowfall. *J. Climate Appl. Meteor.,* **23,** 940–949.

Browning, K. A., A. J. Eccleston, and G. A. Monk, 1985: The use of satellite and radar imagery to identify persistent shower bands downwind of the North Channel. *Quart. J. Roy. Meteor. Soc.,* **114,** 325–331.

Carpenter, D. M., 1993: The lake effect of the Great Salt Lake: Overview and forecast problems. *Wea. Forecasting,* **8,** 181–193.

Cooper, K. A., M. R. Hjelmfelt, R. G. Derickson, D. A. R. Kristovich, and N. F. Laird, 2000: Numerical simulation of transitions in boundary layer convective structures in a lake-effect snow event. *Mon. Wea. Rev.,* **128,** 3283–3295.

Crosman, E. T., and J. D. Horel, 2010: MODIS-derived surface temperature of the Great Salt Lake, 2008. *Remote Sens. Environ.,* **113,** 73–81.

Crum, T. D., R. L. Alberty, and D. W. Burgess, 1993: Recording, archiving, and using WSR-88D data. *Bull. Amer. Meteor. Soc.,* **74,** 645–653.

Hjelmfelt, M. R., 1990: Numerical study of the influence of environmental conditions on lake-effect snowstorms over Lake Michigan. *Mon. Wea. Rev.,* **118,** 138–150.

——, and R. R. Braham, 1983: Numerical simulation of the airflow over Lake Michigan for a major lake-effect snow event. *Mon. Wea. Rev.,* **111,** 205–219.

Holroyd, E. W., 1971: Lake-effect cloud bands as seen from weather satellites. *J. Atmos. Sci.,* **28,** 1165–1170.

Horel, J., and Coauthors, 2002: Mesowest: Cooperative mesonets in the western United States. *Bull. Amer. Meteor. Soc.,* **83,** 211–225.

Kristovich, D. A. R., 1993: Mean circulations of boundary-layer rolls in lake-effect snow storms. *Bound.-Layer Meteor.,* **63,** 293–315.

——, and N. F. Laird, 1998: Observations of widespread lake-effect cloudiness: Influences of lake surface temperature and upwind conditions. *Wea. Forecasting,* **13,** 811–821.

——, and M. L. Spinar, 2005: Diurnal variations in lake-effect precipitation near the western Great Lakes. *J. Hydrometeor.,* **6,** 210–218.

——, N. F. Laird, M. R. Hjelmfelt, R. G. Derickson, and K. A. Cooper, 1999: Transitions in boundary layer meso-γ convective structures: An observational case study. *Mon. Wea. Rev.,* **127,** 2895–2909.

Kusunoki, K., M. Murakami, M. Hoshimoto, N. Orikasa, Y. Yamada, H. Mizuno, K. Hamazu, and H. Watanabe 2004: The characteristics and evolution of orographic snow clouds under weak cold advection. *Mon. Wea. Rev.,* **132,** 174–191.

Laird, N. F., 1999: Observation of coexisting mesoscale lake-effect vortices over the western Great Lakes. *Mon. Wea. Rev.,* **127,** 1137–1141.

——, and D. A. R. Kristovich, 2004: Comparison of observations with idealized model results for a method to resolve winter lake-effect mesoscale morphology. *Mon. Wea. Rev.,* **132,** 1093–1103.

——, ——, and J. E. Walsh, 2003a: Idealized model simulations examining the mesoscale structure of winter lake-effect circulations. *Mon. Wea. Rev.,* **131,** 206–221.

——, J. E. Walsh, and D. A. R. Kristovich, 2003b: Model simulations examining the relationship of lake-effect morphology to lake shape, wind direction, and wind speed. *Mon. Wea. Rev.,* **131,** 2102–2111.

——, J. Desrochers, and M. Payer, 2009a: Climatology of lake-effect precipitation events over Lake Champlain. *J. Appl. Meteor. Climatol.,* **48,** 232–250.

——, R. Sobash, and N. Hodas, 2009b: The frequency and characteristics of lake-effect precipitation events associated with the New York State Finger Lakes. *J. Appl. Meteor. Climatol.,* **48,** 873–886.

——, ——, and ——, 2010: Climatological conditions of lake-effect precipitation events associated with the New York State Finger Lakes. *J. Appl. Meteor. Climatol.,* **49,** 1052–1062.

Lavoie, R. L., 1972: A mesoscale numerical model of lake-effect storms. *J. Atmos. Sci.,* **29,** 1025–1040.

Mesinger, F., and Coauthors, 2006: North American Regional Reanalysis. *Bull. Amer. Meteor. Soc.,* **87,** 343–360.

Murphy, A. H., 1991: Probabilities, odds, and forecasts of rare events. *Wea. Forecasting,* **6,** 302–307.

Niziol, T. A., 1987: Operational forecasting of lake-effect snowfall in western and central New York. *Wea. Forecasting,* **2,** 310–321.

——, W. R. Snyder, and J. S. Waldstreicher, 1995: Winter weather forecasting throughout the eastern United States. Part IV: Lake-effect snow. *Wea. Forecasting,* **10,** 61–77.

Onton, D. J., and W. J. Steenburgh, 2001: Diagnostic and sensitivity studies of the 7 December 1998 Great Salt Lake–effect snowstorm. *Mon. Wea. Rev.,* **129,** 1318–1338.

Passarelli, R. E., and R. R. Braham, 1981: The role of the winter land breeze in the formation of Great Lake snow storms. *Bull. Amer. Meteor. Soc.,* **62,** 482–492.

Payer, M., J. Desrochers, and N. F. Laird, 2007: A lake-effect snowband over Lake Champlain. *Mon. Wea. Rev.,* **135,** 3895–3900.

Steenburgh, W. J., 2003: One hundred inches in one hundred hours: Evolution of a Wasatch Mountain winter storm cycle. *Wea. Forecasting,* **18,** 1018–1036.

——, and D. J. Onton, 2001: Multiscale analysis of the 7 December 1998 Great Salt Lake–effect snowstorm. *Mon. Wea. Rev.,* **129,** 1296–1317.

——, S. F. Halvorson, and D. J. Onton, 2000: Climatology of lake-effect snowstorms of the Great Salt Lake. *Mon. Wea. Rev.,* **128,** 709–727.

U.S. Census Bureau, cited 2011: 2010 Census data. [Available online at http://2010.census.gov/2010census/data/.]

USGS, cited 2012: Great Salt Lake, Utah. [Available online at http://ut.water.usgs.gov/greatsaltlake/.]

Weckwerth, T. M., J. W. Wilson, R. M. Wakimoto, and N. A. Crook, 1997: Horizontal convective rolls: Determining the environmental conditions supporting their existence and characteristics. *Mon. Wea. Rev.,* **125,** 505–526.

Wiggin, B. L., 1950: Great snows of the Great Lakes. *Weatherwise,* **3,** 123–126.

Wood, V. T., R. A. Brown, and S. V. Vasiloff, 2003: Improved detection using negative elevation angles for mountaintop WSR-88Ds. Part II: Simulations of the three radars covering Utah. *Wea. Forecasting,* **18,** 393–403.